

MUON BEAM DYNAMICS AND SPIN DYNAMICS IN THE G-2 STORAGE RING *

D. L. Rubin[†], A. Chapelain, Cornell University, Ithaca, USA

F. Gray, Regis University, Denver, USA

J. Price, S. Charity, University of Liverpool, Liverpool, UK

J. Mott, Boston University, Boston, USA

J. D. Crnkovic, W. Morse, V. Tishchenko, Brookhaven National Laboratory, Upton, USA

W. Wu, University of Mississippi, Oxford, USA

Abstract

The goal of the new g-2 experiment at Fermilab is a measurement of the anomalous magnetic moment of the muon, with uncertainty of less than 140 ppb. The experimental method is to store a beam of polarized muons in a storage ring with pure vertical dipole field and electrostatic focusing, and to measure the precession frequency. Control of the systematics depends on unprecedented knowledge of the details of the phase space of the muon distribution. That knowledge is derived from direct measurements with scintillating fiber detectors that are inserted into the muon beam for diagnostic measurements, traceback straw tube tracking chambers, as well as the calorimeters that measure energy, time and position of the decay positrons. The interpretation of the measurements depends on a detailed model of the storage ring guide field. This invited talk presents results of studies of the distribution from the commissioning run of the experiment.

INTRODUCTION

The muon magnetic moment is a property that can be calculated in the context of the standard model of particle physics. A comparison of the measured and predicted anomaly is a grand test of the model. The goal of the experiment is to measure the anomalous magnetic moment with 140 part per billion precision.

The experimental method is to circulate a beam of polarized muons in a storage ring and to measure the precession frequency, or rather the difference between the precession frequency and the revolution frequency, ω_a , the spin tune. The 3.094 GeV/c momentum muons decay with lifetime of about 64 us in the lab frame to a positron and a pair of neutrinos. The energy of the positron in the lab frame is correlated with the polarization of the parent muon. The variation in the number of high energy positrons with time is the measure of ω_a .

The frequency with which the muons precess depends on the details of the magnetic and electric guide field of the storage ring. Magnetic focusing is evidently precluded as it would introduce an unacceptable variation in the magnetic field across the storage volume. Instead vertical focusing is provided by electrostatic quadrupoles. The muon momentum is chosen to minimize the effect of the electric field

on the precession frequency. Indeed, at the muon magic momentum, 3.094 GeV/c, the contribution of the electric field to the difference frequency vanishes.

We describe the electric and magnetic guide field of the 44.69 m circumference storage ring, the lattice functions and the process for injecting and storing polarized muons. The detector systems that inform the beam distributions are introduced. The contributions to ω_a that arise from finite beam width and length, momentum spread, and coherent oscillation of the centroid are described, as are the measurements of the distributions that are essential to accounting for the effects.

STORAGE RING

The g-2 storage ring is a weak focusing machine with a single adjustable parameter, namely the quadrupole voltage, that determines horizontal and vertical tunes, β -functions, and dispersion. Fig. 1 shows the layout of the ring. The quads [1] are vertically focusing and horizontally defocusing. In the limit where $V_{quad} \rightarrow 0$, the horizontal tune is unity and vertical is zero. With increasing voltage the vertical tune increases and horizontal decreases. Fig. 2 shows horizontal and vertical tunes along the voltage contour. The β and dispersion functions for quad voltage of 20.4 kV are shown in Fig. 3.

The quadrupole field is superimposed on the main dipole field. The reference trajectory through the quadrupoles has significant curvature and the quadrupoles share that curvature. As a result, the quadrupole field is necessarily nonlinear, with a significant sextupole term. An effect of this and other nonlinearities associated with the geometry of the quad electrodes is an amplitude dependence of the tunes. The tunes shifts associated with the various quad multipoles [2] are shown in Fig. 4. The nonlinearities of the electrostatic quadrupoles, as well as residual magnetic multipoles [3] can drive resonances (see Fig. 2). Operation near resonances is avoided to mitigate losses. A tune scan that extends over the operating region is shown in Fig. 5. The storage fraction is measured as quadrupole voltage is increased from 18kV to 23kV. The degraded storage fractions evident at 18.8 kV and 21.2 kV correspond to the $3\nu_x = 1$ and $\nu_x + 3\nu_y = 2$ resonances.

Three distinct detector systems inform the muon distribution. Twenty-four calorimeters [4], distributed uniformly around the inner circumference of the ring, measure en-

* Work supported by DOE DE-SC0008037

[†] david.rubin@cornell.edu

ergy, position and time of decay positrons. There are two tracking stations [5], located 180 and 270 degrees from the injection point, comprised of straw wire chambers, that measure the trajectory of the decay positron. The reconstructed track is then traced back to reveal the position of the parent muon. The fiber harp system provides the most direct measure of the circulating muons. Each of the four harps consists of seven 0.5mm diameter parallel scintillating fibers with 13mm spacing. There are two horizontal and two vertically oriented harps at 180 and 270 degrees respectively. The fiber harps [6] are rotated into the beam to measure time dependence of beam centroid and profile, and are retracted during production running.

The guide field is characterized by measurements of closed orbit, tunes, and modulation of the beam width and centroid. Measurements of the tunes with the fiber harps are shown in Fig. 2. The fiber harps and the tracking detectors provide complimentary measurements of motion of the centroid (Figs. 6 and 7) and modulation of the width, Fig. 8.

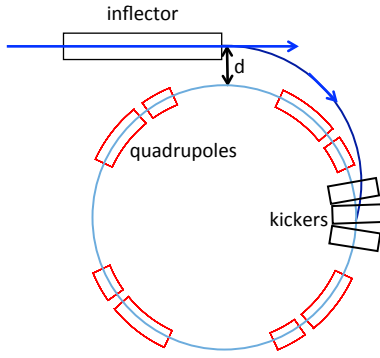


Figure 1: Injected beam enters the g-2 ring through a hole in the backleg iron. It emerges from the backleg and enters the inflector which cancels the field of the storage ring magnet. Beam exits the inflector, and enters the ring through the kicker gap. The circumference of the ring is 44.69 m (revolution period 149 ns). The 1.45 T bending field is continuous around the ring.

INJECTION

The beam is injected into the ring through a hole in the backleg iron. The 1.7m long superconducting inflector bucks the main dipole field so that the beam traverses the inflector without significant deflection and exits the inflector on a trajectory tangent to a displaced circular orbit. The beam crosses the design orbit in the gap of the pulsed kicker that steers the beam radially outward and onto the central orbit as shown in Fig. 1.

The inflector aperture (18 mm horizontally by 56 mm vertically) is very much smaller than the aperture of the ring (90mm round). In order to maximize transmission, the beam is focused to a narrow waist through the inflector and with zero dispersion.

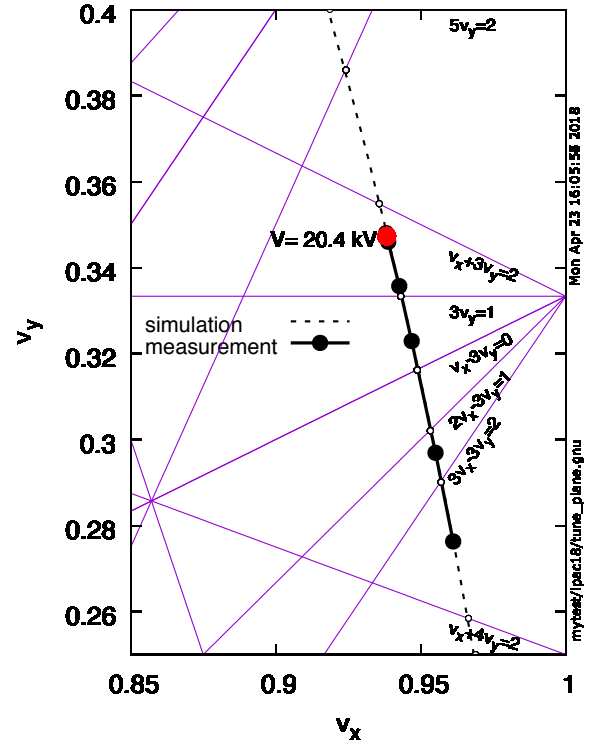


Figure 2: Dependence of tune on quadrupole voltage computed with a BMAD [7] based model of the guide field. Resonance lines are shown. Tentative operating point is 20.4 kV (red dot).

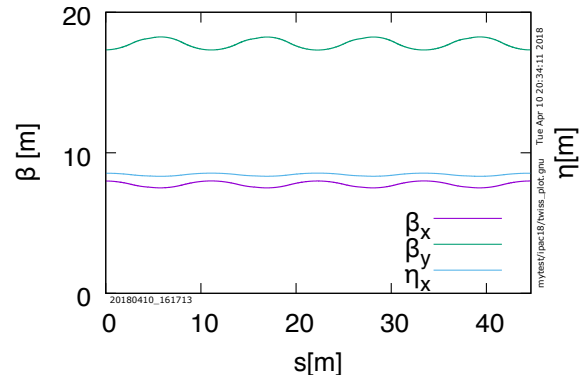


Figure 3: Twiss parameters in the closed storage ring

Manipulation of the beam width to maximize transmission through the inflector and into the ring is illustrated in Fig. 9. The mismatch of dispersion and β -functions leads to a modulation of beam width with components at the betatron frequency and twice the betatron frequency respectively. The relative contribution of betatron motion and momentum offset to the width can be extracted from the width measurement (Fig. 8) by suitable decomposition.

The kicker is located $\phi_\beta = \pi/2$ downstream from the injection point at the inflector exit. The beam crosses the design orbit with an angle determined by the radial displace-

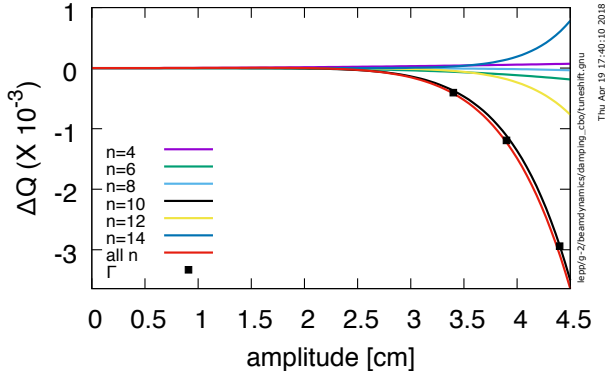


Figure 4: Simulated contribution to amplitude dependent tune shift from each of the quad multipoles, their sum, and the decoherence rate Γ as determined by tracking.

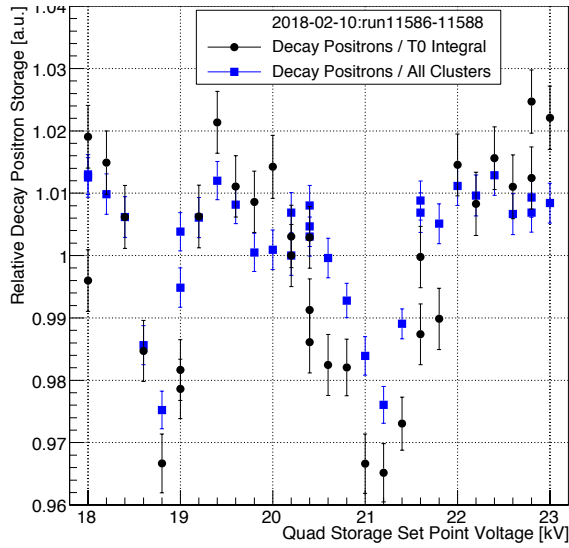


Figure 5: Relative number of decay positrons in a fill as a function of quadrupole voltage. The number of positrons is a proxy for the number of stored muons. Storage efficiency is degraded by betatron resonances at 18.8 kV and 21.2 kV.

ment of the inflector axis (nominally 77 mm from the design orbit and indicated as 'd' in Fig. 1), and the exit angle. The crossing angle, and therefore the kick required to steer the beam onto the closed orbit, is minimum if the exit angle is zero. The dependencies can be made quantitative with a few simplifying assumptions, namely that the β and η functions are uniform around the ring, and as long as we treat the kickers as a δ -function in azimuthal angle. (The kickers [8] in fact extend over about 36 deg of arc). With these assumptions, the horizontal displacement of the trajectory is

$$\begin{aligned} x(s) &= (x_{inf} - \delta\eta) \cos(\phi(s)) + \eta\delta \\ &\quad - k\beta_0 \cos \phi(s) + x'_{inf} \sin \phi(s) \\ &= A \cos(\phi(s) + \phi_0) + \eta\delta \end{aligned}$$

where x_{inf}, x'_{inf} are the displacement and angle of the trajectory at the inflector exit, η the dispersion, δ is the frac-

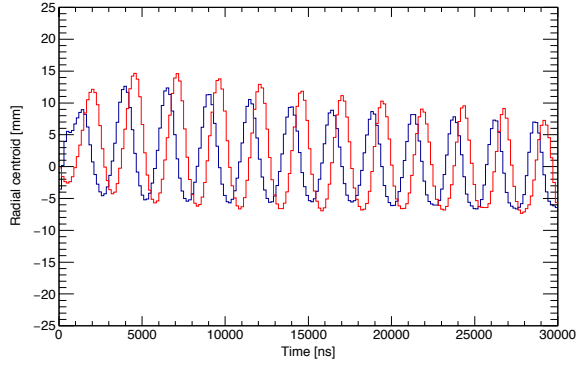


Figure 6: Horizontal position of centroid measured with the 180 deg fiber harp (blue) and 270 deg harp (red) for the first 30 μ s of the fill. An FFT yields the horizontal tune.

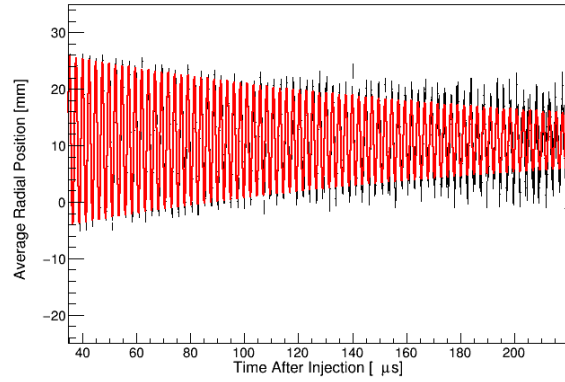


Figure 7: Radial centroid as measured with the 180 deg tracker over the first 220 μ s of the fill. Red curve is a fitted damped sinusoid. Measurement is increasingly noisy at longer times as statistics are limited.

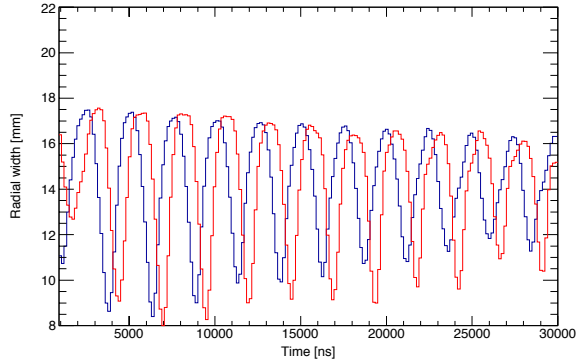


Figure 8: Horizontal width at 180 degree harp (blue) and 270 deg harp (red) over the first 30 μ s of the fill. The deep modulation is a combination of dispersive and β mismatch.

tional momentum offset, k is the kick angle, $\phi(s)$ the betatron phase advance with $s = 0$ at the injection point, $A = \pm \sqrt{(x_{inf} + \delta\eta - k\beta)^2 + (x'_{inf}\beta)^2}$ and $\tan \phi_0 = \frac{x'_{inf}\beta}{x_{inf} - \delta\eta - k\beta}$. The extremes of the displacement of the

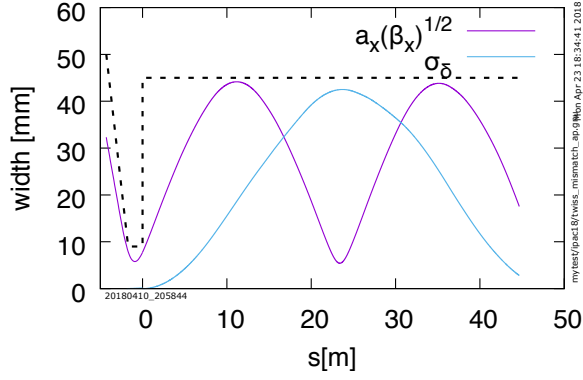


Figure 9: Propagating beam betatron and energy width through narrow aperture inflector and into the storage ring. The dashed line is the horizontal aperture

motion, that is the envelope of the motion is given by $x_{ext} = \pm|A| + \eta\delta$. The envelope is plotted in Fig. 10 as a function of momentum for three different injection angles, and for a kick angle $k = 8\text{ mrad}$, which is about 80% of the nominal kick, and Fig. 11 for the nominal kick of $k = 10.8\text{ mrad}$. The minimum momentum that can be stored decreases as the kicker angle approaches nominal. Under-kicking skews the momentum distribution high. Kick and injection angle both contribute to the amplitude of the oscillations about the closed orbit. Non zero injection angle reduces momentum acceptance symmetrically about zero.

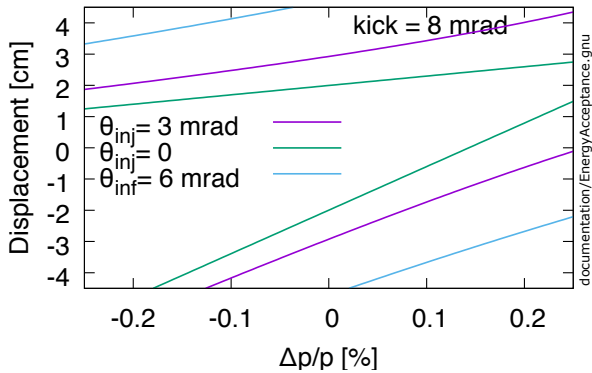


Figure 10: Kick angle $\sim 80\%$ of nominal. The green lines mark the envelope of the motion of a muon that exits the inflector with zero angle. The on momentum muon oscillates between $\pm 2\text{ cm}$. If momentum offset is 0.2% the peak to peak oscillation is $\sim 5\text{ mm}$. A muon with momentum offset of -0.18% is outside the 4.5 cm aperture.

SYSTEMATICS

The expression for the anomalous precession frequency, in the limit of vanishing longitudinal magnetic field, is

$$\vec{\omega}_a = -\frac{q}{m} \left[a_\mu \vec{B} - a_\mu \left(\frac{\gamma}{\gamma+1} \right) (\vec{\beta} \cdot \vec{B}) \right]$$

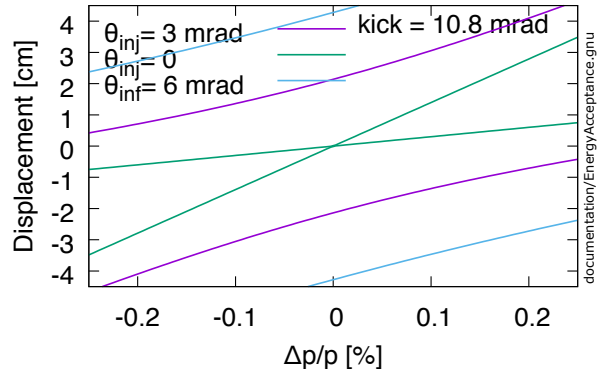


Figure 11: For the nominal kick angle (10.8 mrad), the trajectory of the on momentum muon coincides with the closed orbit. The on momentum muon injected with angle of $\pm 3\text{ mrad}$ will oscillate within a $\pm 2\text{ cm}$ envelope.

$$-\left(a_\mu - \frac{1}{\gamma^2 - 1} \right) \frac{\vec{\beta} \times \vec{E}}{c} \quad (1)$$

For muons at magic momentum ($p_{mag} = m/\sqrt{a_\mu}$) circulating on the design orbit, $\vec{\omega}_a = -\frac{q}{m} a_\mu \vec{B}$.

Pitch correction

Vertical oscillations will contribute to our measurement of the anomalous precession through the second term in Eq. 1, the so-called pitch correction. The measured distribution of vertical phase space is used to compute the size of the effect. A fiber harp measurement of the vertical width over the first $30\mu\text{s}$ of the fill is shown in Fig. 12.

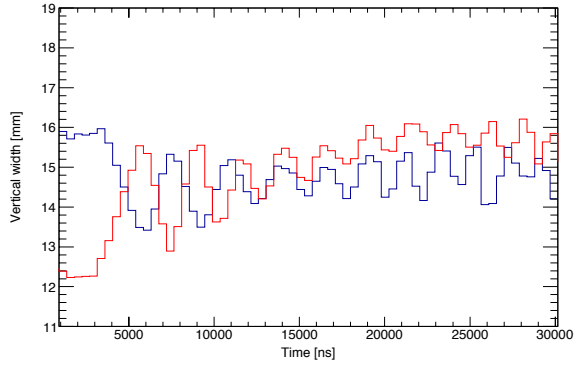


Figure 12: Evolution of the vertical width.

E-field correction

The E-field systematic is associated with the third term on the right hand side of Eq. 1 and scales with momentum offset and radial electric field. The electric field depends in turn on transverse displacement. Estimating the size of the E-field systematic depends on measurement of the momentum and the radial distribution. The radial distribution is measured directly with fiber harps and trackers, albeit with somewhat different acceptances. The momentum distribution is determined by a “fast rotation analysis”, that

exploits the connection between the revolution frequency and the momentum. A technique [9] based on Fourier transform yields a frequency spectrum that can be correlated with radius (circumference) and momentum. An alternative method extracts the momentum distribution from the measured debunching of the muon beam. The fast rotation data is provided by the calorimeters which measure the time dependence of the intensity of the distribution. Examples of frequency distribution extracted by the Fourier method and radial distribution via the debunching analysis are shown in Fig. 13 and 14 respectively. A radial distribution measured with the traceback detector is shown in Fig. 15. Comparison of the radial distribution extracted from the fast rotation data and the traceback trackers requires some care as acceptances are very different. All data are preliminary.

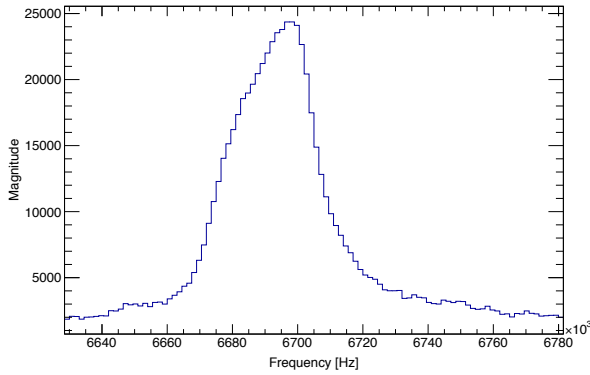


Figure 13: Fourier analysis of the fast rotation signal gives the muon revolution frequency spectrum. Higher frequency corresponds to lower momentum and smaller radius. The revolution frequency of the magic momentum muon is 6.7 MHz.

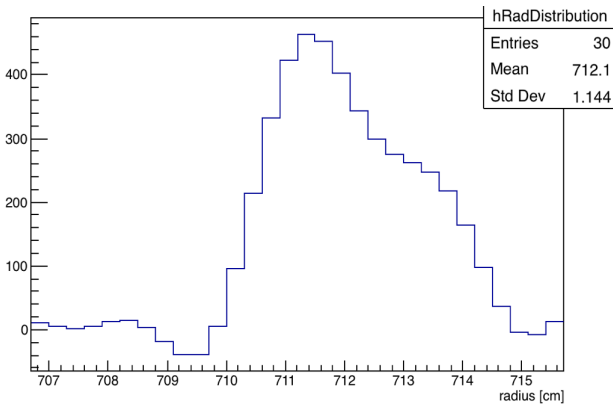


Figure 14: The radial distribution is determined by analysis of the debunching in the fast rotation signal (preliminary). The radius of the magic momentum muon is 711.2 cm.

Acceptance and coherent motion

The acceptance of the calorimeters for the decay positron depends on the radial position of the parent muon. The acceptance therefore varies as the centroid of the distribution oscillates and the width is modulated over the course of the fill. The coherent motion of the centroid, that results from

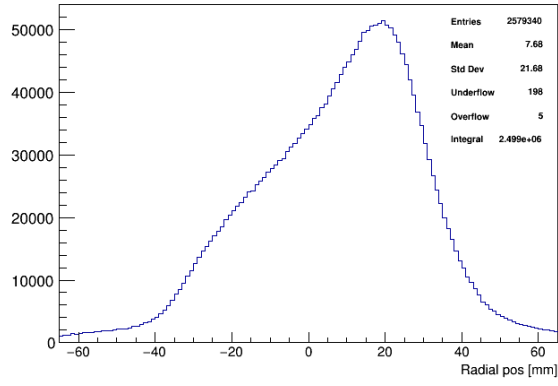


Figure 15: Radial position of decay muon measured with traceback tracking station. (Preliminary data.)

errors in injection angle and kicker field, and the coherent modulation of the beam width, arising from the phase space mismatch at injection, are characterized by decoherence times. (The coherent motion and modulation early in the fill is evident for example in Fig. 6 and 8, and the decoherence at later times in Fig. 7). The beam decoheres because of the amplitude and momentum dependence of tunes associated with quadrupole nonlinearity (discussed above) and the chromaticity. But the leading source of decoherence is the large momentum spread and the strong dependence of path length on momentum. The change in circumference due to fractional momentum offset is $\frac{\Delta C}{C} \sim \frac{\eta}{R} \frac{\Delta p}{p} \Rightarrow \Delta p/p$ in the weak focusing limit. The momentum acceptance of the ring is $\Delta p/p \sim \pm 0.125\%$. The distribution will lap itself in as few as four hundred turns or $60 \mu s$, effectively mixing the distribution. Indeed a measure of the decoherence time is an indication of the width of the momentum distribution.

CONCLUSION

A quantitative understanding of the evolution of the muon distribution over the course of the fill is essential to limiting the systematic uncertainty in the measurement of the anomalous magnetic moment to the 70 ppb (systematic) target. The experiment is equipped with detectors that can measure phase space and momentum distribution in some detail, as we have demonstrated with a few examples. Beam dynamics simulations informed by the measurements complete the description. The preliminary data presented above was collected during the commissioning phase of the experiment. Nevertheless it is clear that the fiber harp and tracker systems are an extraordinary window on the behavior of the circulating distribution.

ACKNOWLEDGEMENT

We thank E989 Collaborators, the Fermi National Accelerator Laboratory, a U.S. Department of Energy, Office of Science, HEP User Facility for the resources provided. Fermilab is managed by the Fermi Research Alliance, LLC(FRA), acting under Contract No. DE-AC02-07CH11359. The authors are supported by the US NSF, and the UK STFC. I also wish

to thank all of our colleagues who made this experiment and these measurements possible and with whom I have benefited from countless discussions.

REFERENCES

- [1] J.D.Crnkovic, “Commissioning the Muon g-2 Experiment Electrostatic Quadrupole System”, presented at the 2018 Int. Particle Accelerator Conf. (IPAC’18), Vancouver, Ca, Ma 2017, paper WEPAF015 ,this conference
- [2] Y. Semertzidis, et al., “The Brookhaven muon (g-2) storage ring high voltage quadrupoles” *Nucl. Instr. Meth. A*, vol. 503, pp. 458-484, 2003.
- [3] J. Grange et al.,” Muon g-2 Technical Design Report”, FERMILAB-DESIGN- 2014-02, arXiv:1501.06858, p. 281
- [4] J. Grange et al.,” Muon g-2 Technical Design Report”, FERMILAB-DESIGN- 2014-02, arXiv:1501.06858, p. 525
- [5] J. Grange et al.,” Muon g-2 Technical Design Report”, FERMILAB-DESIGN- 2014-02, arXiv:1501.06858, p. 575
- [6] J. Grange et al.,” Muon g-2 Technical Design Report”, FERMILAB-DESIGN- 2014-02, arXiv:1501.06858, p. 611
- [7] D. Sagan, “Bmad: A relativistic charged particle simulation library,” *Nucl. Instr. Meth. A*, vol. 558, pp. 356–359, 2006.
- [8] A. P. Schreckenberger et al.,”New Fast Kicker Results from the Muon g-2 E-989 Experiment at FERMILAB”, presented at the 2018 Int. Particle Accelerator Conf. (IPAC’18), Vancouver, Ca, Ma 2017, paper THPML093, this conference
- [9] J. Grange et al.,” Muon g-2 Technical Design Report”, FERMILAB-DESIGN- 2014-02, arXiv:1501.06858, p. 575
- [9] Yuri Orlov, Cenap S. Ozben, and Yannis K. Semertzidis, “Muon revolution frequency distribution from a partial-time fourier transform of the g-2 signal in the muon g-2 experiment”*Nucl. Instrum. Methods Phys. Res. A*, 482:9, 2002.